



## ORIGINAL ARTICLE

# Size, surface charge and flexibility of vinegar-baked Radix Bupleuri polysaccharide affecting the immune response



Xiaoshuang Wang<sup>a,b,1</sup>, Ya Zhao<sup>a,b,1</sup>, Yayun Wu<sup>a,b,d</sup>, Lijuan Liu<sup>a,b</sup>, Minjie Liang<sup>f</sup>, Minghui Han<sup>a,b</sup>, Ping Li<sup>b</sup>, Ziqing Chen<sup>c</sup>, Hongbing Yan<sup>c</sup>, Ruizhi Zhao<sup>a,b,d,e,\*</sup>

<sup>a</sup> The Second Clinical Medical School of Guangzhou University of Chinese Medicine, China

<sup>b</sup> The Second Affiliated Hospital of Guangzhou University of Chinese Medicine, China

<sup>c</sup> School of Chinese Materia Medica of Guangzhou University of Chinese Medicine, China

<sup>d</sup> Guangdong Provincial Key Laboratory of Clinical Research on Traditional Chinese Medicine Syndrome, China

<sup>e</sup> State Key Laboratory of Dampness Syndrome of Chinese Medicine, The Second Affiliated Hospital of Guangzhou University of Chinese Medicine, China

<sup>f</sup> School of Traditional Chinese Medicine, Guangdong Pharmaceutical University, China

Received 12 January 2022; accepted 23 May 2022

Available online 27 May 2022

## KEYWORDS

Vinegar-baked *Radix Bupleuri*;  
Polysaccharide;  
Nanoparticle;  
Structure;  
Immune-enhance

**Abstract** Remarkably, nanomaterials can interact with the cells of immune system and either enhance or inhibit its function in many ways. Unfortunately, such valuable information has been overlooked in studies of polysaccharide immune activity. This study isolated a nano-polysaccharide from vinegar-baked *Radix Bupleuri* by membrane separation system, DEAE-52 and Sephadex-G200. The physicochemical characterization and immunoregulatory activity were studied through DLS, Congo red, Scanning Electron Microscope, UV-Vis, HPGPC, FT-IR, Methylation, NMR, MTT, neutral red and enzyme linked immunosorbent assay. Results showed that VBCP2.5 was an acidic polysaccharide with a molecular weight of 674 kDa. Its monosaccharides composed of mannose, rhamnose, galacturonic acid, glucose, galactose and arabinose at a molar ratio of 1.72: 9.59: 57.63: 5.37: 6.71: 18.99. VBCP2.5 possessed micelle forming ability at 25.574  $\mu\text{g}/\text{mL}$  and flexible chain conformation, as well as with a small size distribution ~

\* Corresponding author at: The Second Affiliated Hospital of Guangzhou University of Chinese Medicine, Inner Ring West Road, Guangzhou Higher Education Mega Center, Guangzhou, 510006, China.

E-mail addresses: 1447952375@qq.com (X. Wang), 13423631120@163.com (Y. Zhao), 659984113@qq.com (Y. Wu), liulijuan@gzucm.edu.cn (L. Liu), lmj13544560021@163.com (M. Liang), h13544555760@163.com (M. Han), 908679518@qq.com (P. Li), 1471948179@qq.com (Z. Chen), 1471948179@qq.com (H. Yan), 13610241754@163.com (R. Zhao).

<sup>1</sup> These authors contributed equally to this work.

Peer review under responsibility of King Saud University.



Production and hosting by Elsevier

84.99 nm and positive charge in stimulated blood fluid and different from that in deionized water. The microtopography was characterized by irregular lamellar, dendritic, cylindrical or spherical aggregates, with folds and cracks on the surface. Structure analyses showed that VBCP2.5 characterized by high proportion of 1,4 linked- $\alpha$ -D-GalpA and a small fraction of RG-I, some other glycosidic linkages included 1,5 linked- $\alpha$ -L-Araf, 1,3,5 linked- $\alpha$ -L-Araf, 1,3,4 linked-Galp, 1,4,6 linked-Manp, t- $\alpha$ -L-Araf, t- $\beta$ -D-Glcp and t- $\alpha$ -D-Galp were also comprised. VBCP2.5 exhibited immunomodulatory potential which included the promotion of phagocytosis, the release of NO and the secretion of TNF- $\alpha$  and IL-6 of RAW264.7 cells. The possible activation of macrophages by VBCP2.5 may be mediated through endocytosis pathway. Small size, positive charge, shape and flexible conformation may accelerate this process. The information gathered here could lead to new platform for comprehensive understand included primary structure, properties of nanoscale, and correlation with immunoregulation of polysaccharides.

© 2022 The Author(s). Published by Elsevier B.V. on behalf of King Saud University. This is an open access article under the CC BY-NC-ND license (<http://creativecommons.org/licenses/by-nc-nd/4.0/>).

## 1. Introduction

As we all know, the immune system protects the host from a variety of pathogenic microorganisms (Parkin and Cohen, 2001). Various diseases and treatments are major causes of immunocompromise (Cant and Cole, 2010). Immunocompromised and immunosuppressive individuals are more sensitive to infection (Weber and Rutala, 2003). There are myriad examples that underscore the gravity of the impact infectious diseases have had on humans such as the black death, smallpox, measles, diarrhoeal disease, influenza and other devastating infectious diseases (Toamih et al., 2018). All these cause various forms of disabilities and death especially in developing nations, afflicting more than one billion people and costing developing nations billions of dollars year after year, besides incalculable wounds inflicted on the sufferers (Nii-Trebi, 2017). It is estimated that at least 25% of about 60 million deaths each year are due to infectious diseases worldwide (Fauci et al., 2005). Immunopotentiators can regulate the immune function and are often used in the prevention and treatment of infectious diseases (Medina, 2016). Clinical commonly used immunopotentiators include thymosin, interferon, colony-stimulating factor, interleukin, pitomodulate, transfer factors, bacterial agents and others (Fang-bo et al., 2017). But there are some adverse reactions such as rash, nausea, vomiting, headache, dizziness and so on (Lihong, 2015).

Nanomedicine is traditionally used to describe a 1 ~ 1000 nm sized drug delivery systems, which was widely used in various diseases. The use of nanomaterials themselves to active immune response is an area that has recently sparked significant interest (Lasola et al., 2020). Nanoparticles are usually easily recognized as foreigners from body by macrophages, triggering an immune response. Composition, shape, size, and physicochemical properties of the nanomaterials play critical roles in influencing the immune system response. They can interact with the cells of the immune system in many different ways (Toma et al., 2018). However, engineered nanoparticles may induce inflammation and immunotoxicity (Khan et al., 2019).

Polysaccharides are biopolymers which characterized by good biocompatibility, non-toxicity, hydrophilily and biodegradability, making them more preferred as ideal biomaterials for the synthesis of nanoparticles (Liu et al., 2008). Beyond that, polysaccharides possess broad bioactivities and

are more suitable candidates for good medicines (Xie et al., 2016). Unfortunately, most studies focus their research either on the application of polysaccharides as biomaterials or their bioactivity and primary structure as drug (Zhao et al., 2020). The correlation between their inherent immunostimulatory activity and nano-properties of polysaccharides are generally lacking. Furthermore, with the development of molecular biology, the scientific community has gradually realized that polysaccharides, together with proteins and polynucleotides, are extremely important biomacromolecules. They display properties that cannot only be attributed to the monomers but are also associated with their complex secondary and tertiary structure (Torres et al., 2019). It's reported that the aggregation generated a more potent form with augmented response in immune cells than soluble form (Serrano-Sevilla et al., 2019). Therefore, it is necessary to conduct a comprehensive study on its nano-properties, shape, conformation, structure and bioactivity.

Traditional Chinese herbs are main source of immunostimulatory polysaccharides (Wenbo et al., 2015). Radix Bupleuri is a traditional Chinese medicine which derives from the dry root of *Bupleurum chinense* DC. and *Bupleurum scorzoneri-folium* Willd; has played an important role in health care and disease treatment in many countries (Sun et al., 2019). It is not only used to treat diseases such as abdominal pain, chest swelling and food accumulation, but also in health care products, cosmetics, daily necessities industry and other fields, such as slimming tea, health wine, ointment for dispelling nevus, soap and health cigarette etc. (Jiang et al., 2020). Modern pharmacology has proved that Radix Bupleuri has anti-inflammatory and immunomodulatory effects (Feiwu et al., 2020). Polysaccharides are main active ingredients that are receiving more and more attention (Li et al., 2019). Previously, it has been reported that Radix Bupleuri crude polysaccharides could up-regulate phagocytic activity in inflammatory disease and inhibit the production of NO and pro-inflammatory cytokines induced by LPS (Cheng et al., 2010). Processing is the most common method in Chinese medicine, which can improve therapeutic effect of natural Chinese herbal medicine, and more suitable for clinical application (Xueqin et al., 2018).

In this study, we purified a homogeneous polysaccharide from Vinegar-baked Radix Bupleuri (VBRB) through a membrane separation system, DEAE-52 and Sephadex-G200. Nano-properties in normal and simulated physiological environment, conformation, microtopography, structure and

immunoregulatory activity of VBCP2.5 were studied. We aim to provide VBCP2.5 a list of dynamic physicochemical properties in nano scale and primary structure parameters that may have contributed to the immunoregulatory activity and made recommendations on future studies attempting to correlate the nano-properties of polysaccharides and the immune responses induced.

## 2. Materials and methods

### 2.1. Materials and reagents

Vinegar-baked radix bupleuri was purchased from Kangmei Medica Company (Guangzhou, China), and certified as genuine by Wenliang Chen, deputy director of the Second Affiliated Hospital of Guangzhou University of Chinese Medicine. RAW264.7 cells were purchased from China center for type culture collection (Wuhan, China). DMEM medium, Fetal bovine serum (FBS) and Penicillin Streptomycin were supplied by GIBCO (USA). Nitric Oxide (NO) assay kit was purchased from Jiancheng Bioengineering Institute (Nanjing, China). Enzyme-linked immunosorbent assay (ELISA) kits for TNF- $\alpha$  and IL-6 were purchased from Elabscience (Wuhan, China). Thiazolyl Blue (MTT) and Dimethyl sulfoxide (DMSO) were purchased from MP Biomedicals, LLC (France). Lipopolysaccharide was purchased from Jingxin Biological Technology Co., Ltd (Guangzhou, China). Monosaccharide standards were purchased from Yuanye Biotechnology Co., Ltd (Shanghai, China). Dextran standards were purchased from American Polymers Standards Corporation (USA).

### 2.2. Isolation and purification of VBCP2.5

Extraction of crude polysaccharides was performed according to the previous protocol (Zhao et al., 2020). Briefly, VBRB powders were degreased with 70% ethanol. The crude polysaccharides were extracted with boiling water and precipitated by 80% ethanol at 4 °C overnight. Proteins were removed by Sevage method. The crude polysaccharides solution was filtered by a membrane separation system equipped with UFP-750-E-4MA and UFP-100-C-4MA hollow fiber columns (general electric company, USA). The filtered sample was loaded on a DEAE Sepharose Fast Flow column (2.6 × 80 cm), then successively eluted with water, 0.025, 0.1, 0.2, 0.4, 0.8 and 1.0 mol/L NaCl at a rate of 5 mL/min. All fractions were collected in line with measured OD values at 490 nm that represented the total carbohydrate detected by the phenol-sulfuric acid method. The main fraction (0.4 M NaCl) referred to as VBCP2.5 was further eluted with water on a Sephadex G-200 column (1.6 × 90 cm) at a rate of 0.3 mL/min.

#### 2.2.1. Ultraviolet scanning

Polysaccharide solution (500  $\mu$ g/mL) was put in a quartz cuvette and scanned ranging from 400 nm to 200 nm on a U-2910 ultraviolet spectrophotometer (Hitachi Hi-Tech Co, Japan).

#### 2.2.2. Homogeneity and molecular weight distribution

Samples were analyzed by HPGPC method on an Agilent 1200 HPLC system equipped with RID detector and a TSKgel G5000PWXL column (7.8 mm × 300 mm, Tosoh

Corporation, Japan). Deionized water was used as mobile phase and passed through the column at a flow rate of 0.4 mL/min, and the column temperature was set as 40°C. The standard curve was established by standard dextrans (2400 K, 820 K, 400 K, 215 K, 95 K, 50 K).

#### 2.2.3. Compositional analysis

Carbohydrate content was determined by the phenol-sulfuric acid method using D-galacturonic acid as a standard (Ruibin et al., 2017). Protein content was detected according to Pierce<sup>TM</sup> BCA Protein Assay Kit (Thermo, USA). Uronic acid content was assessed by m-hydroxybiphenyl method (Yaping and Hongli, 2019); and galacturonic acid was used as a standard. The endotoxin content was detected by Tachypleus Limulus Endotoxin Testing Kit (Xiamen Bioendo Technology Co., Ltd, China).

### 2.3. Micelle forming ability

The polysaccharide solution was irradiated with a laser to observe whether the Tyndall effect occurred. 80  $\mu$ l pyrene acetone solution (6.0 mg/L) was put into a brown penicillin bottle and volatilized with N<sub>2</sub>. VBCP2.5 solution (2, 1, 0.5, 10<sup>-1</sup>, 10<sup>-2</sup>, 10<sup>-3</sup>, 10<sup>-4</sup>mg/mL) was added to each bottle, the mixtures were sonicated for 30 mins, then keep in a water bath at 60°C for 3 h, finally incubated at 40°C overnight. Fluorescence spectra of each solution were scanned using an Infinite M1000Pro (Tecan, Switzerland) at 25°C, the excitation wavelength was set as 333 nm, the bandwidth was 5.0 nm and the emission spectrum range from 350 to 450 nm. Linear regression equation was fitted according to the ratio of I<sub>1</sub> (373 nm) to I<sub>3</sub> (384 nm) and the logarithm of concentration.

### 2.4. Size and charge analysis

Samples of VBCP2.5 were dissolved in deionized water or simulated bloodfluid (DMEM medium, 10% FBS, pH~7.4), for 0 h, 1 h and 24 h, at a thermostatic incubator, to investigate their behavior in conventional and physiological conditions. 0.8  $\mu$ m of polyether sulfone filter membranes were used to remove residues before the test. Dynamic light scattering (DLS) experiments were performed using a Nano SizerZeter Brookhaven Instrument (Nanobrook 90Plus PALS, USA), operating at 640 nm. Samples were diluted in Polystyrene cell monitored according to the manufacturer's instructions. Results were analyzed by soft of Particle Solutions v.3.6.07122.

### 2.5. Shape observation

Dried polysaccharides were fixed on a conductive adhesive and then sputtered with gold powder. The surface characteristics and microstructure were observed using a Hitachi SU8000 series Scanning Electron Microscope (Tokyo, Japan) at a 5.0 KV acceleration voltage.

### 2.6. Conformation in solution

The polysaccharide sample (2 mg/mL in water) was first equally mixed with Congo red solution (0.2 mM). NaOH solution (1 M) was then added to produce a series of solutions with

a final NaOH concentration (0 M, 0.05 M, 0.1 M, 0.15 M, 0.2 M, 0.3 M, 0.4 M). The maximum absorption wavelength of the mixtures was determined on a U2910 UV spectrophotometer ranging from 200 to 800 nm (Wu et al., 2018).

## 2.7. Structural characterization

### 2.7.1. Infrared spectrum analysis

The overdried polysaccharide was recorded on an FT-IR spectrophotometer (Spectrum Two, PerkinElmer, USA) in a frequency range of 4000–400  $\text{cm}^{-1}$ .

### 2.7.2. Monosaccharide composition analysis

VBCP2.5 (5 mg) was hydrolyzed with 5 mL 2 M trifluoroacetic acid (TFA) at 110 °C for 6 h and derivatized by PMP (Zhang et al., 2016). The derivative was analyzed on an Agilent 1260 equipped with diode array detector (DAD) and Diamonsil C18 column (250 × 4.6 mm, 5  $\mu\text{m}$ ). The whole process was monitored at 254 nm and the column temperature controlled at 30 °C. The mobile phase was composed of 50 mM phosphate buffer solution (pH = 6.85) in a percentage of 83 and acetonitrile in a percentage of 17, eluted at a flow rate of 1.0 mL/min.

### 2.7.3. Methylation analysis

**2.7.3.1. Carboxyl reduction.** VBCP2.5 was reacted with N-(3-Dimethylaminopropyl)-N'-ethylcarbodiimide hydrochloride (EDC) at room temperature for 3 h, the pH was controlled at 4.75 by 0.1 M HCl. And then 2 M of sodium borohydride ( $\text{NaBH}_4$ ) was added slowly to the reaction mixture at room temperature, and the reaction continued for 2 h, the pH was controlled at 7.0 by 4 M HCl. The solution was dialyzed (molecular weight cut-off 3.5 kd) in water for 48 h. The whole process was repeated thrice.

**2.7.3.2. Methylation.** The overdried carboxyl-group reduced samples were dissolved in 4 mL anhydrous DMSO in a round bottom flask filled with  $\text{N}_2$  and sonicated at 40 °C. Then, a suspension of NaOH/DMSO was injected into the solution and sonicated for 1 h under the temperature condition between 18 ~ 20 °C. The methylation reaction was initiated by the addition of 1.5 mL  $\text{CH}_3\text{I}$  and lasted for 0.5 h at room temperature. The mixture was extracted with 2 mL  $\text{CHCl}_3$  partitioned against deionized water (3 ~ 5 mL) three times. Then the permethylated product was pre-hydrolyzed in formic acid (88%) for 4 h and completely hydrolyzed in 2 M TFA for 6 h. The hydrolyzed product was reduced with  $\text{NaBH}_4$  for 4 h at room temperature and then acetylated with acetic anhydride-pyridine (1:1) at 95°C for 1 h. Finally, the partially methylated alditol acetates (PMAAs) were analyzed by GC-MS, using an Agilent HP-5MS capillary column (0.25 × 250  $\mu\text{m}$ , 30 m). Samples were injected in a splitting ratio of 8:1 and PMAAs were separated using a temperature program consisting of an initial isothermal period (150 °C for 2 min) followed by a linear increase (2.5 °C/min) to 250 °C (held for 20mins).

### 2.7.4. NMR spectroscopic analysis

VBCP2.5 (50 mg) was dissolved in 0.5 mL  $\text{D}_2\text{O}$  and freeze-dried for 3 times, then redissolved in 0.5 mL  $\text{D}_2\text{O}$  and inspected on a Bruker 600 MHz NMR spectrometer at 25°C.

## 2.8. Immune activity assay of VBCP2.5 in RAW264.7 cells

### 2.8.1. Cell viability assay

RAW264.7 cells were cultured in DMEM medium containing 10% FBS and 1% Pen & Strep, kept in an incubator at 37°C with 5%  $\text{CO}_2$ . A MTT method was used to determine the cell viability. Raw264.7 cells were seeded in 96-well plate at a density of  $1 \times 10^4$  cells/well. VBCP2.5 (62.5, 31.25, 15.6  $\mu\text{g}\cdot\text{mL}^{-1}$ ) were added to wells and LPS (2.5  $\mu\text{g}/\text{mL}$ ) as control. After stimulation for 24 h, 20  $\mu\text{l}$  of MTT solution (5 mg/mL) was added and incubated for 4 h, the supernatant was replaced with 150  $\mu\text{l}$  of DMSO. The plate was measured at 490 nm on a microplate reader (Infinite M1000Pro, Tecan Switzerland).  $\text{Viability}\% = \text{OD}_1/\text{OD}_0 \times 100\%$ , where  $\text{OD}_0$  is the absorbance of the control and  $\text{OD}_1$  is the absorbance of the sample.

### 2.8.2. Determination of phagocytosis

The phagocytosis was measured by the uptake of neutral red (Tang et al., 2019). Briefly, RAW264.7 cells ( $2 \times 10^4$  cells/well) were seeded in 96-well plates and then stimulated with polysaccharides for 24 h. After that, the supernatant was replaced with 100  $\mu\text{l}$  of 0.1% neutral red solution and incubated for 0.5 h, cells were washed by PBS. At last, 100  $\mu\text{l}$  of cell lysis solution (ethanol/acetic acid, 50:1, v/v) was added to each well and incubated overnight. OD value was measured at 540 nm and phagocytosis rate was calculated as follow equation:  $\text{Phagocytosisrate}\% = \text{OD}_e/\text{OD}_c \times 100\%$ , where “e” represents the experiment group and “c” represents the control group.

### 2.8.3. NO, TNF- $\alpha$ and IL-6 detection

Different concentrations of VBCP2.5 and LPS were added to stimulate the cells for 24 h. After that, the supernatant was collected for NO, TNF- $\alpha$  and IL-6 assay which performed according to the instructions of kits.

## 2.9. Statistical analysis

Data were expressed as the mean  $\pm$  standard deviation (SD). One-way analysis of variance was used. A *p*-value of <0.05 was considered statistically significant.

## 3. Results

### 3.1. Purity and chemical composition analysis

The yield of crude polysaccharides was 56.16%, polysaccharides filtered by a membrane separation with a yield of 36.43%, the fraction of 0.4 M NaCl eluted through DEAE Sepharose Fast Flow column with a yield of 60.72%, the purified polysaccharide (VBCP2.5) obtained from the Sephadex G-200 column with a yield of 76.90% (Fig. 1A, B). The results of UV-Vis showed that there were no obvious convex peaks at 280 nm and 260 nm, indicating that no protein or nucleic acid in VBCP2.5 (Fig. 1D and Table. 1). As shown in Fig. 1C, the HPGPC profiles indicated that VBCP2.5 with a relatively single molecular feature. According to the regression equation of dextran standards, the  $M_w$  of VBCP2.5 was calculated to be 674 kDa. The carbohydrate content was 95.89% and uronic acid content was 57.19%. The endotoxin content in sample

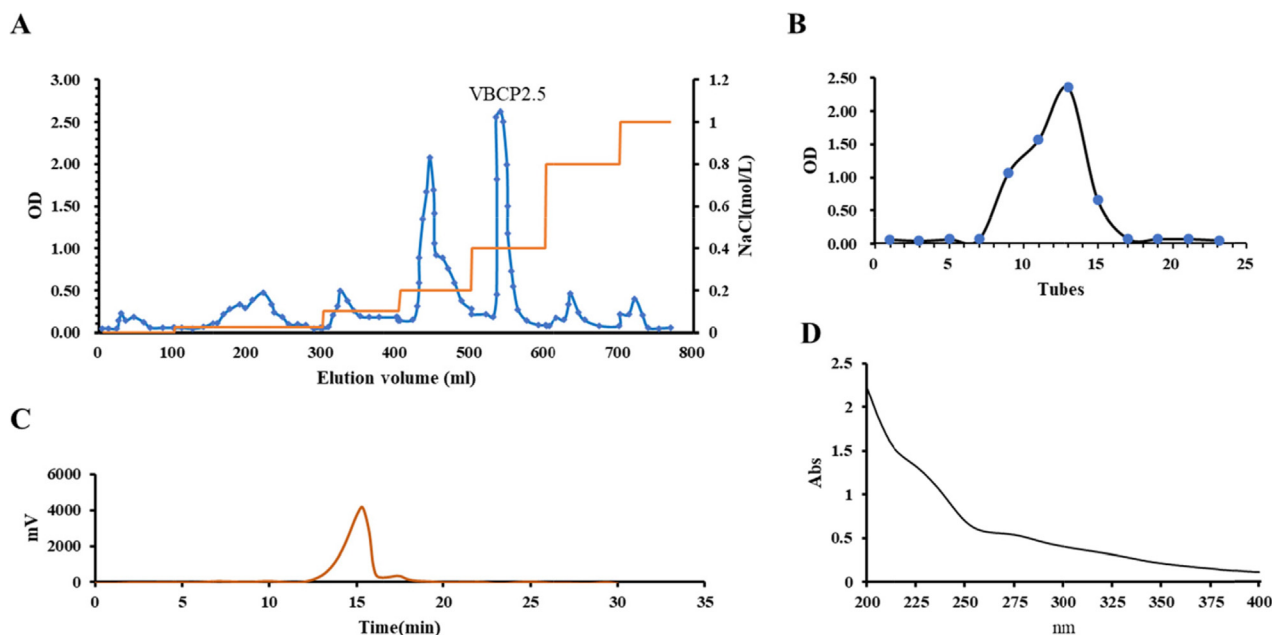


**Fig. 1** Isolation and purification of VBCP2.5 from vinegar-baked Radix Bupleuri and its characterization. **A.** Elution curve on DEAE-FF; **B.** Elution curve on G200; **C.** HPGPC chromatogram of VBCP2.5; **D.** Ultraviolet scanning spectrum of VBCP2.5 (400 ~ 200 nm).

**Table 1** The chemical composition of VBCP2.5.

Component	Content	Equation
Total carbohydrate (%)	95.89%	$y = 0.0014x + 0.012, r^2 = 0.99$
Protein (%)	not detected	$y = 0.001x + 0.1146, r^2 = 0.996$
Uronic acid (%)	57.19	$y = 8.3279x - 0.0087, r^2 = 0.999$
Molecular weight (kDa)	674	$t = -7.3514\text{Log}(Mw) + 58.127, r^2 = 0.99$
Endotoxin (EU)	$0.56 < 1.5$	$y = 1.6973x + 0.7754, r^2 = 0.99$

was determined by a Tachypleus Limulus Endotoxin Testing Kit. The 5 ng/mL LPS used in the assay was equivalent to approximately 1.09 EU/mL endotoxin. Our results show that when the concentration of VBCP2.5 is 1000  $\mu\text{g/mL}$ , the endotoxin content is only 0.56 EU/mL.

### 3.2. Tyndall effect and critical micelle concentration analysis

An obvious Tyndall phenomenon was observed in VBCP2.5 solution (Fig. 2 A) which indicated the formation of colloidal. The critical micelle concentration experiment further proved this (Fig. 2 B), and the critical micelle concentration was calculated as 52.574  $\mu\text{g/mL}$  based on the intersection of two regression straight lines ( $y_1 = -0.4564x + 1.1821$ ;  $y_2 = 0.002x + 1.7685$ ).

### 3.3. Particle size and potential analysis

As shown in Fig. 3, a  $314.40 \pm 11.14$  nm size of VBCP2.5 with a polydispersity (PDI) of  $0.35 \pm 0.02$  in deionized water was detected. After incubation 1 h at 37°C, the major size distribution was shifted to  $352.60 \pm 4.84$  nm. When the incubation time extended to 24 h, the size mainly distributed near by  $146.40 \pm 11.08$  nm with a PDI of  $0.35 \pm 0.02$ . When VBCP2.5 incubated in simulated bloodfluid (DMEM medium,

10% FBS, pH~7.4) at 37°C for 0 h, 1 h, 24 h, it characterized by a small and stable size of  $84.99 \pm 3.27$  nm, PDI of  $0.32 \pm 0.02$ ,  $83.241.53$  nm, PDI of  $0.33 \pm 0.01$ , and  $91.27 \pm 4.26$  nm, PDI of  $0.29 \pm 0.02$ . Negative values of zeta potential were measured in samples include VBCP2.5 (0 h, 1 h, 24 h in H<sub>2</sub>O) and VBCP2.5 (0 h in simulated bloodfluid), which recorded as  $-31.83 \pm 9.98$  mV,  $-28.91 \pm 5.36$  mV,  $-56.82 \pm 1.43$  mV,  $-35.73 \pm 13.35$  mV respectively. However, in the presence of simulated bloodfluid (1 h and 24 h of incubation), VBCP2.5 exhibited positive charges of  $25.25 \pm 9.25$  mV and  $14.53 \pm 0.43$  mV.

### 3.4. Microtopography analysis

As shown in Fig. 4 A, irregular lamellar, dendritic, cylindrical or spherical shapes were observed at 1000 times, obvious spherical particles and closely connected particles were seen at 15,000 times local magnification (Fig. 4 B), and obvious protrusions and folds were observed at 20,000 times further magnification (Fig. 4 C).

### 3.5. Conformation analysis

Congo red can form a complexity with polysaccharides that have a triple-helix structure. In a certain range of NaOH con-

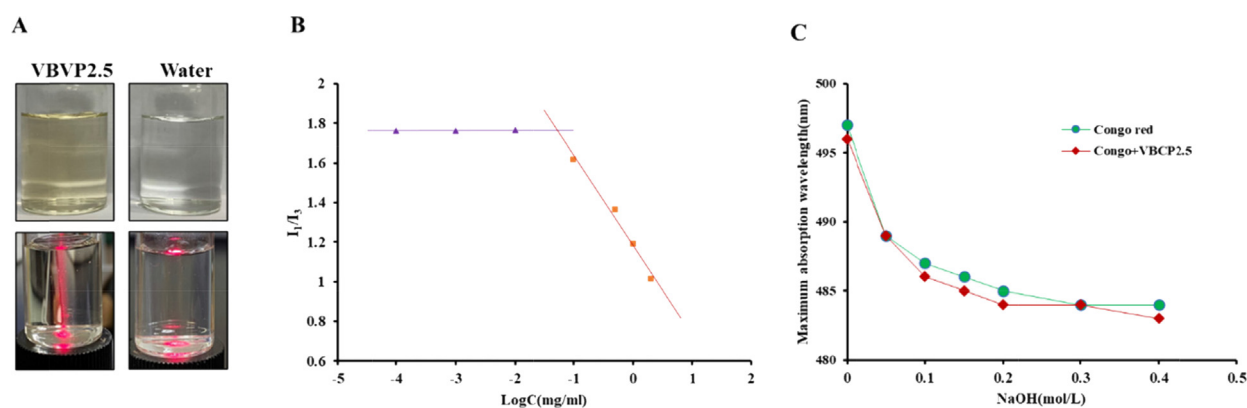


**Fig. 2** VBCP2.5 exhibited micellar properties but not a triple helix configuration in solution. **A**, Tyndall effect in water solution of VBCP2.5, **B**, Critical micelle concentration curve of VBCP2.5; **C**, Maximum absorption wavelength of congo red solution with and without VBCP2.5 at different concentrations of NaOH.

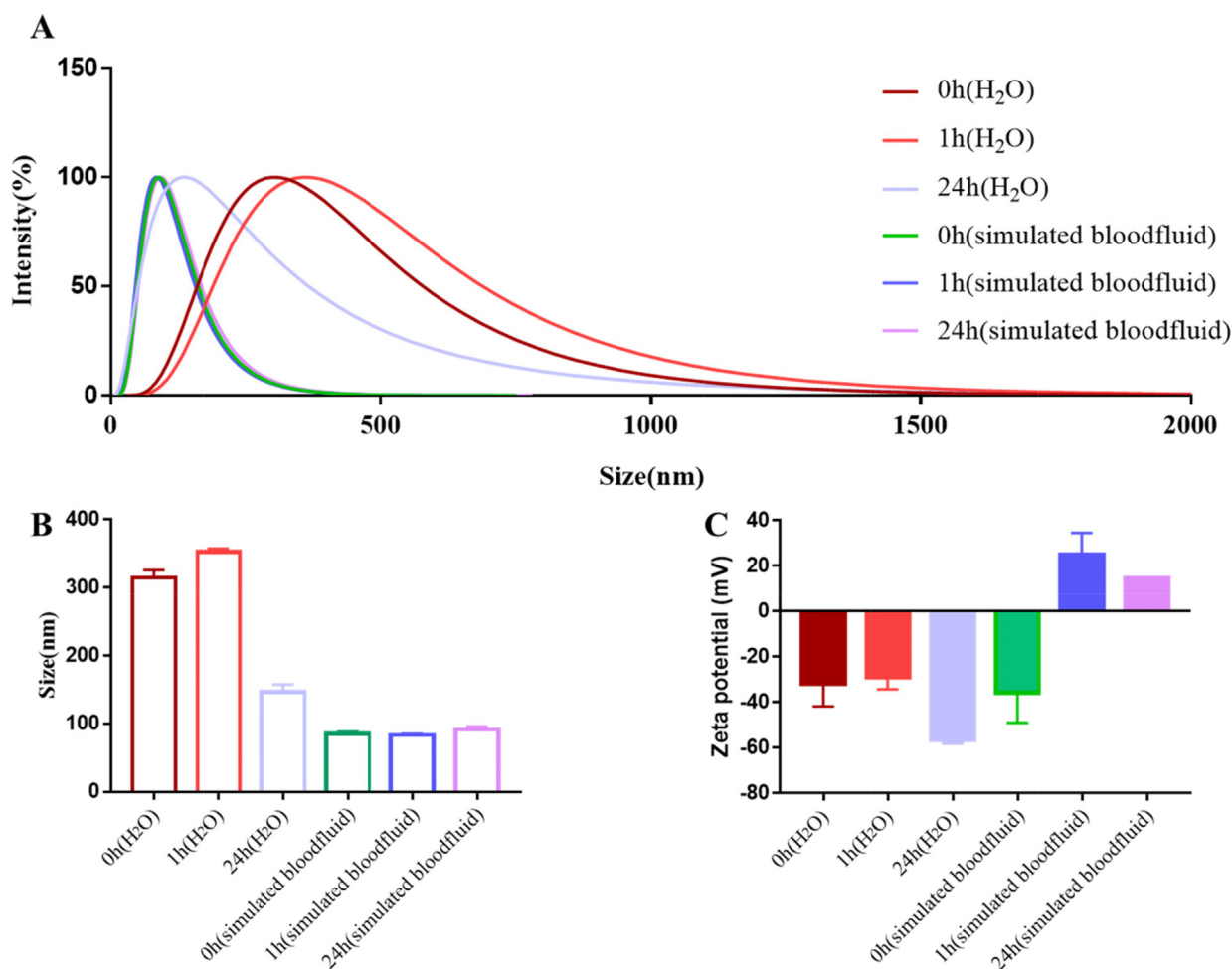


**Fig. 3** Size and surface chemistry characterization of VBCP2.5. **A**, Intensity-weighted size distribution of VBCP2.5 in H<sub>2</sub>O or simulated bloodfluid (1 and 24 h of incubation); **B**, Size mean values; **C**, Zeta potential mean values.

centration, the maximum absorption wavelength of the complex is bathochromic shifted compared with that of the Congo red (Zhang et al., 2017). As shown in Fig. 2 C; as the concen-

tration increasing of NaOH at 0 ~ 0.4 mol/L, the maximum absorption wavelengths of both Congo red and Congo red + VBCP2.5 solution gradually declined, and the trend

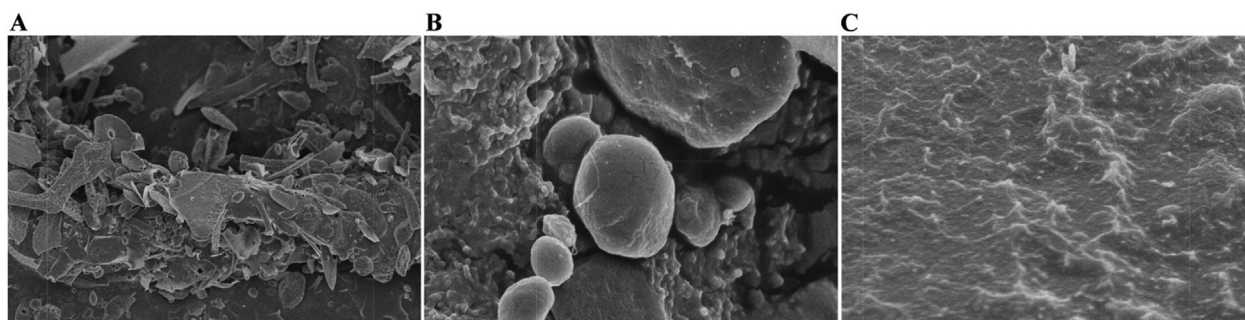


**Fig. 4** Scanning Electron Microscopy (SEM) images of VBCP2.5 at different scales. (A. 1000 $\times$ ; B. 15000 $\times$ ; C20000  $\times$ ).

was similar. At the same time, no obvious phenomenon of bathochromic shift was observed during the experiment, indicating that VBCP2.5 did not form a complex with Congo red, and did not have a triple-helix structure.

### 3.6. Structural analysis

#### 3.6.1. FT-IR analysis

As shown in Fig. 5 A, the broad and strong characteristic peak at 3309  $\text{cm}^{-1}$  represents O-H stretching vibration, while 2948  $\text{cm}^{-1}$  was attributed to C-H stretching vibration. The 1600 and 1411  $\text{cm}^{-1}$  bands came from carboxylate groups (Wilson et al., 2000). The absorbance peaks at 1475–1300  $\text{cm}^{-1}$  were assigned to the vibrations of C-H and represented the deformations of  $\text{CH}_2$  groups. The absorbance peaks at 1200–1000  $\text{cm}^{-1}$  were assigned to the contribution of C-OH or C-O-C stretching vibration. Near 1100–1010  $\text{cm}^{-1}$ , three observable absorption peaks indicated that VBCP2.5 was a pyranose.

#### 3.6.2. Monosaccharide composition

The standard monosaccharides spectrum of HPLC was shown in Fig. 5 B, serial numbers 1 to 8 respectively represented mannose(Man), ribose(Rib), rhamnose(Rha), glucuronic Acid (GluA), galacturonic Acid(GalA), glucose(Glc), galactose (Gal) and arabinose(Ara). The results showed that VBCP2.5 was composed of Man, Rha, GalA, Glc, Gal and Ara at a molar ratio of 1.72: 9.59: 57.63: 5.37: 6.71: 18.99 (Fig. 5 D).

#### 3.6.3. Methylation analysis

GC-MS spectrum of methylated alditol acetates was shown in Fig. 5 C. Based on CCRC Spectral Database (<https://www.ccr.edu/specdb/ms/pmaa/pframe.html>), GC-MS local mass spectra database NIST14 and related literature (Xia et al., 2020; Padmanabhan and Shah, 2020; He et al., 2017; Gan et al., 2020); the linkage patterns of VBCP2.5 were summarized in Table. 2. As the polysaccharide had been reduced before methylation, the residues of galacturonic acid (GalpA) were presented as galactose residues (Galp). There were nine

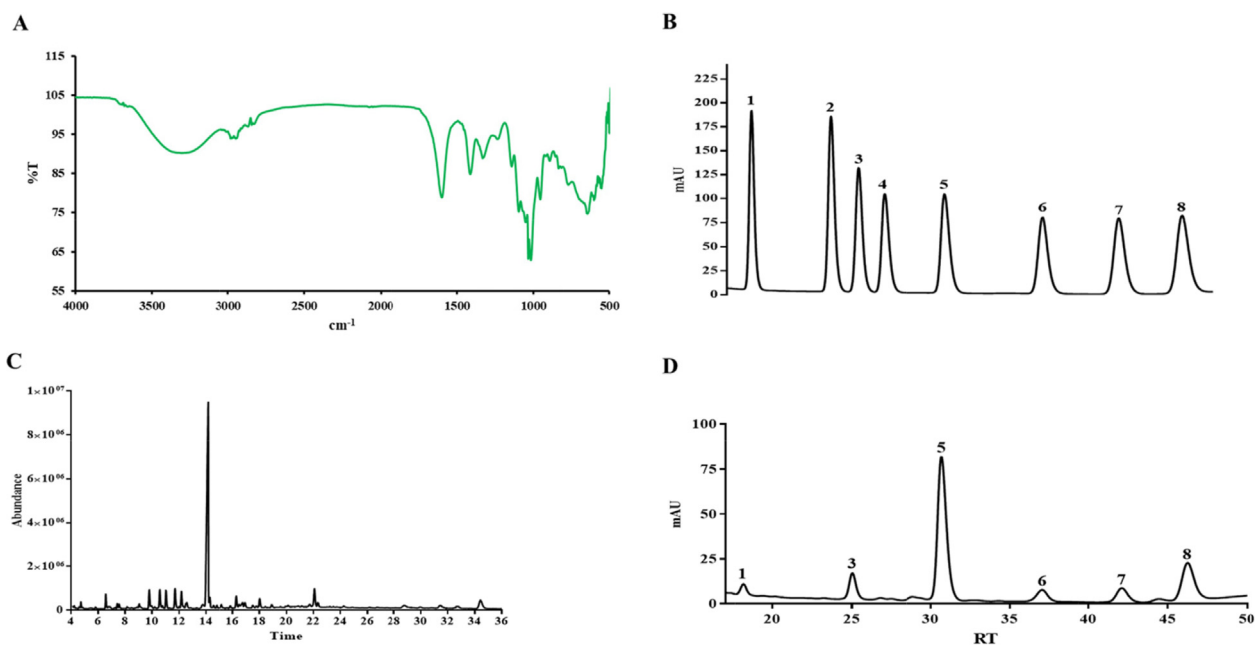


**Fig. 5** Structural characterization of VBCP2.5. A. Infrared spectrogram of VBCP2.5; B and D. HPLC profile of monosaccharide composition (1, Man; 2, Rib; 3, Rha; 4, GlcA; 5, GalA; 6, Glc; 7, Gal; 8, Ara). C. GC-MS spectrum of methylated alditol acetates.

**Table 2** Glycosidic linkage type analysis of VBCP 2.5.

Rt (min)	Methylated residues	Linkage type	Area percent (%)	Mass fragment (m/z)
6.57	2,3,5-tri- <i>O</i> -methyl-arabinitol	t linked-Araf	2.16	117, 43, 129, 101, 161, 87, 71, 102
9.79	2,3-di- <i>O</i> -methyl-arabinitol	1,5 linked-Araf	3.29	117, 43, 129, 101, 87, 89, 99, 189
10.56	3,4-di- <i>O</i> -methyl-mannitol	1,2 linked-Rhap	3.85	87, 43, 202, 117, 101, 131, 216, 89, 229
11.02	2,3,4,6-tetra- <i>O</i> -methyl-glucitol	t linked-Glcp	3.80	101, 43, 117, 161, 129, 145, 87, 205, 71
11.69	2,3,4,6-tetra- <i>O</i> -methyl-galactitol	t linked-Galp	4.64	117, 43, 101, 129, 145, 161, 87, 205, 71
12.18	2- <i>O</i> -methyl-arabinitol	1,3,5 linked-Araf	3.90	117, 43, 85, 127, 99, 87, 159, 261, 58
14.13	2,3,6-tri- <i>O</i> -methyl-galactitol	1,4 linked-Galp	63.21	117, 43, 113, 233, 101, 99, 87, 129, 131
16.32	2,6- <i>O</i> -methyl-galactitol	1,3,4 linked-Galp	2.54	117, 43, 129, 87, 143, 97, 185, 115
18.04	2,3-di- <i>O</i> -methyl-D-mannitol	1,4,6 linked-Manp	2.32	117, 43, 127, 101, 85, 261, 99, 87, 129

main sugar linkages in reduced VBCP2.5, including t linked-Araf, 1,5 linked-Araf, 1,2 linked-Rhap, t linked-Glcp, t linked-Galp, 1,3,5 linked-Araf, 1,4 linked-Galp, 1,3,4 linked-Galp and 1,4,6 linked-Manp at an area percent of 2.16, 3.29, 3.85, 3.80, 4.64, 3.90, 63.21, 2.54, 2.32. More details about the information for each of the derivatives identified were shown in **Fig. S1**.

### 3.6.4. NMR analysis

The structure characteristics of VBCP2.5 were analyzed by NMR spectra. 1D NMR spectra ( $^1\text{H}$  NMR and  $^{13}\text{C}$  NMR) and 2D NMR spectra (HSQC, HMBC and  $^1\text{H}$ - $^1\text{H}$  COSY) were shown in **Fig. 6**. Carbon and hydrogen signals assignment were listed in **Table 3**. In  $^{13}\text{C}$  NMR spectra, the signal at  $\delta$ 174.83 ppm indicated the presence of uronic acid, signal of 16.62 was the characteristic of C6 of Rhap (Xu et al., 2011). In  $^1\text{H}$  NMR spectra, seven signals were observed and marked with A-H1(4.84), B-H1(5.61), C-H1(4.93), D-H1(4.39), E-H1(5.10), F-H1(5.03) and G-H1(4.88). In HSQC spectra, cross peaks of B(107.28/5.61), C(106.93/4.93), A(98.95/4.84), E(92.00/5.10), D(95.92/4.39) and G(4.88/107.45) at anomeric region were observed. According to the proportion of monosaccharides composition, glycosidic linkages of methylation and literature, residues of B, C, A, D, E and G were assigned as C1/H1 of (1,5)- $\alpha$ -L-Araf (Cardoso et al., 2002), t- $\alpha$ -L-Araf (Cardoso et al., 2002); (1,4)-D-GalpA (Stone et al., 2014), t- $\beta$ -D-Glcp (Wang and Guo, 2020; Zhang et al., 2016), (1,2)- $\alpha$ -L-Rhap (Zhang et al., 2020) and (1,3,5)- $\alpha$ -L-Araf (Zeng et al., 2020) respectively. In  $^1\text{H}$ - $^1\text{H}$  COSY spectra, correlation peaks of 4.84/3.58, 3.58/3.79 and 3.79/4.20 were thus assigned as H1/H2, H2/H3 and H3/H4 of residue A. Signal at 4.60 was assigned as H5 by a correlation peak of 4.60/174.77(H5/C6) in HMBC. Based on  $^1\text{H}$ - $^1\text{H}$  COSY,  $\delta_{\text{H}}$  at 4.39 ppm, 3.30 ppm and 3.54 ppm were assigned as H1, H2 and H3 respectively, the corresponding carbon chemical shifts were assigned based on HSQC spectra. Other signals were too weak to be accurately attributed. In  $^1\text{H}$ - $^1\text{H}$  COSY, correlation peaks of 5.10/3.80 and 3.54/1.05 were assigned as H1/H2 and H5/H6 of residue E. Signals of 5.03 and 3.77 were classified as H1 and H3 of t- $\alpha$ -D-Galp(F) by reference (Shi et al., 2021), and the rest signal were not fully identified due to the low responses and overlapping signals. Signal of 4.07 was correlated with 5.61 in  $^1\text{H}$ - $^{13}\text{C}$  COSY spectra, which was recognized as H2 of residue B. A weak correlation peak (5.61/70.33) was observed in HBMC, which could be assigned as H5 of (1, 5)- $\alpha$ -L-Araf. H4 was assigned by the correlation of

H4/H5 in  $^1\text{H}$ - $^1\text{H}$  COSY. In  $^{13}\text{C}$  NMR spectra, signal at 60.51 ppm was identified as C5 of  $\alpha$ -L-Araf (Cardoso et al., 2002), the cross peak of 3.51/60.51 was observed in HSQC, correlation peak of 4.07/3.51 and 4.93/4.09 were attributed to H4/H5 and H1/H2 in  $^1\text{H}$ - $^1\text{H}$  COSY. Chemical shifts at 83.71 ppm and 67.87 ppm were classified as C3 and C5 of (1,3,5)- $\alpha$ -L-Araf. Other signals were assigned same as above mentioned. The glycosidic sequences of residues were analyzed through HMBC spectra. In HMBC, the correlation peak of 4.20/98.95(A-H4/A-C1) and 5.61/70.33(B-H1/B-C5) indicated repeat units of 1,4 linked  $\alpha$ -D-GalpA and 1, 5 linked- $\alpha$ -L-Araf. Other weak correlation peaks 4.85/70.33(A-H1/B-C5), 4.85/81.75(A-H1/E-C2), 4.93/83.71(C-H1/G-C3) and 5.03/107.28(F-H1/B-C1) suggested that the O-1 of residue A was linked to C-5 of residue G, the O-1 of residue A was linked to C-2 of residue E, the O-1 of residue C was linked to C-3 of residue G, the O-1 of residue F was linked to C-1 of residue B.

Considering the literature (Mohnen, 2008) and results of FT-IR, monosaccharide composition, methylation and NMR spectra analysis, possible major primary structure of VBCP2.5 was drawn as shown in **Fig. 6 F**. The backbone of VBCP2.5 might be composed of high proportion of 1,4 linked- $\alpha$ -D-GalpA and a small fraction of RG-I. Besides, 1,5 linked- $\alpha$ -L-Araf as side chain attached to the backbone, and terminal saccharides included t- $\alpha$ -L-Araf, t- $\beta$ -D-Glcp and t- $\alpha$ -D-Galp.

### 3.7. Immunity analysis

#### 3.7.1. VBCP2.5 exhibited nontoxic effect on RAW 264.7 cells

Macrophages play a vital role in the innate and adaptive immunity response. Herein, the cytotoxicity effect of VBCP2.5 on macrophages was evaluated by MTT assay. As shown in **Table 4**, after being treated with VBCP2.5 (62.5, 31.25, 15.63  $\mu\text{g}/\text{mL}$ ), the cell viabilities were 103.1%, 109.7% and 118.8% respectively. Results suggested that VBCP2.5 had no significant suppressive effect to the viability of RAW264.7 cells ( $p > 0.05$ ) compared with the control group.

#### 3.7.2. Effect of VBCP2.5 on the phagocytosis of RAW264.7 cells

Neutral red uptake is often used to estimate macrophage phagocytosis. Results showed that the cells treated with 62.5, 31.25, and 15.63  $\mu\text{g}/\text{mL}$  of VBCP2.5 had significantly ( $p < 0.001$ ) greater phagocytosis rates than those treated with the control (**Table 4**).

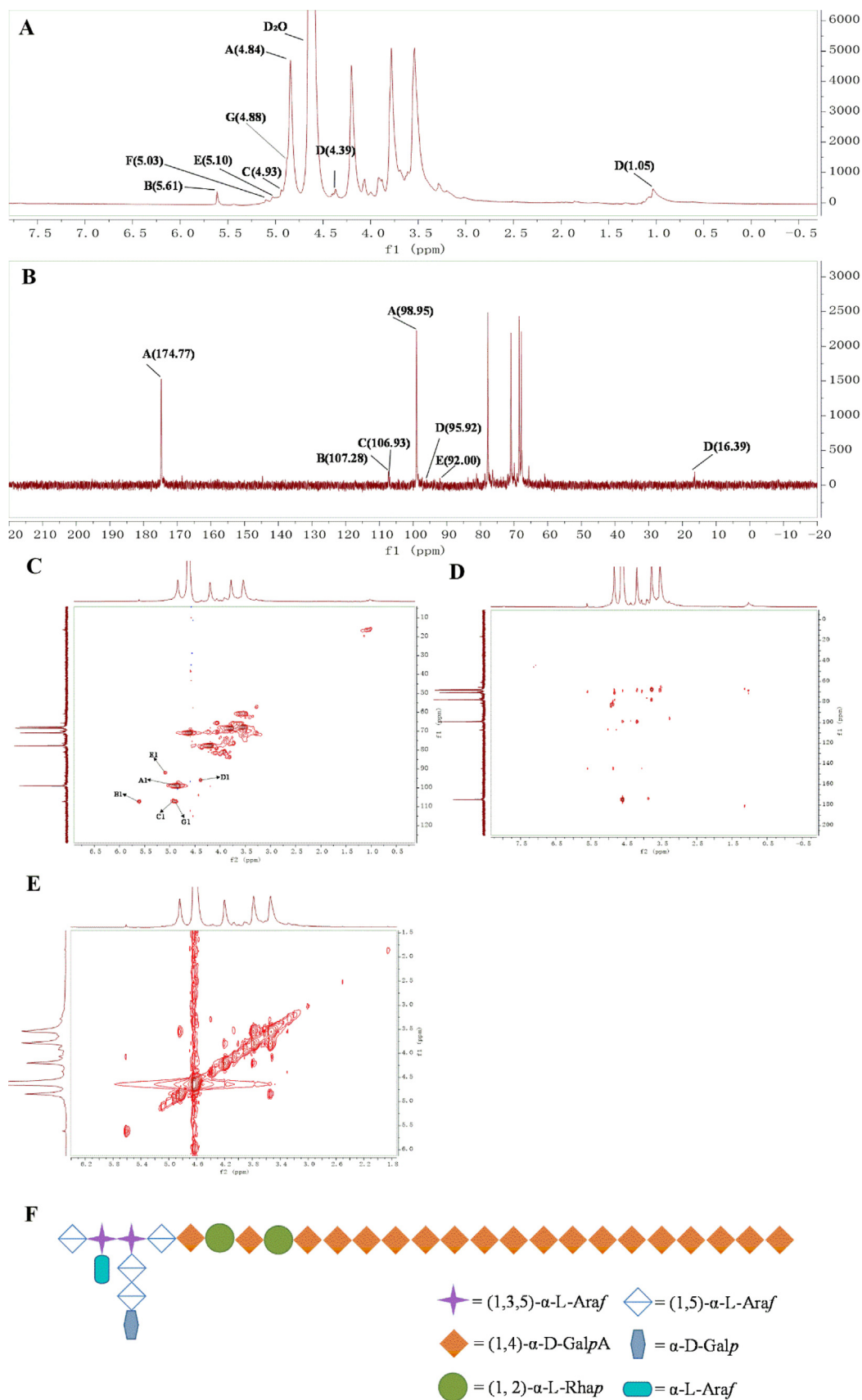


**Fig. 6** NMR spectrum of VBCP2.5. **A.**  $^1\text{H}$  NMR; **B.**  $^{13}\text{C}$  NMR; **C.**  $^1\text{H}$ - $^{13}\text{C}$  HSQC; **D.** HMQC; **E.**  $^1\text{H}$ - $^1\text{H}$  COSY; **F.** The primary structure of VBCP2.5. (“A”, 1,4 linked- $\alpha$ -D-GalpA; “B”, 1,5 linked- $\alpha$ -L-Araf; “C”, t- $\alpha$ -L-Araf; “D”, t- $\beta$ -D-Glcp; “E”, 1,2 linked- $\alpha$ -L-Rhap; “F”, t- $\alpha$ -D-Galp; “G”, 1,3,5 linked- $\alpha$ -L-Araf).

**Table 3** Summary of  $^1\text{H}$  and  $^{13}\text{C}$  NMR chemical shifts of VBCP2.5.

Residues	H1/C1	H2/C2	H3/C3	H4/C4	H5/C5	H6/C6
(1,4)- $\alpha$ -D-GalpA	4.84/98.95	3.58/72.01	3.79/68.48	4.20/77.76	4.60/70.90	-/174.77
(1,2)- $\alpha$ -L-Rhap	5.10/92.00	3.80/81.75	–	–	3.54/	1.05/16.62
t- $\alpha$ -D-Galp	5.03/-		3.77/-			–
(1, 5)- $\alpha$ -L-Araf	5.61/107.28	4.07/80.93	–	4.00/82.02	3.53/70.33	
t- $\alpha$ -L-Araf	4.93/106.92	4.09/81.45		4.07/78.95	3.51/60.51	
(1,3,5)- $\alpha$ -L-Araf	4.88/107.45	4.22/81.45	3.82/83.71	4.02/82.02	3.55/67.87	
t- $\beta$ -D-Glcp	4.39/95.92	3.28/71.18	3.54/72.01	-/-	-/-	

“–”, not assigned.

**Table 4** Effect of VBCP2.5 on cytotoxicity and phagocytosis rate in RAW264.7 cells.

Group	Dosage ( $\mu\text{g/mL}$ )	Viability (%)	Phagocytosis rate (%)
Control		102.2 $\pm$ 6.53	100 $\pm$ 11.21
VBCP2.5	62.5	103.1 $\pm$ 14.32	135.2 $\pm$ 7.37***
	31.25	109.7 $\pm$ 6.545	145.2 $\pm$ 5.15***
	15.63	118.8 $\pm$ 3.195	143.1 $\pm$ 11.14***

Note: Data were presented as mean  $\pm$  SD; \*\*\* $p$  < 0.001, compared to the control group.

### 3.7.3. VBCP2.5 promote the release of NO

As shown in Fig. 7 A, by comparison with the control group, NO levels were significantly elevated by LPS stimulation ( $p$  < 0.001). Interestingly, VBCP2.5 also significantly increased NO levels ( $p$  < 0.001) when it was administered at 62.5, 31.25, and 15.63  $\mu\text{g/mL}$ . Especially, the high dose of VBCP2.5 was greater than LPS. Results showed that VBCP2.5 markedly stimulated macrophage NO production in a dose-dependent manner.

### 3.7.4. Cytokine secretion increased after VBCP2.5 stimulation

As shown in Fig. 7 B and C, LPS stimulation significantly increased the secretion of TNF- $\alpha$  and IL-6 compared to the control group ( $p$  < 0.01). VBCP2.5 promoted the secretion of TNF- $\alpha$  in a dose-dependent manner ( $p$  < 0.05), and the secretion of IL-6 was also significantly increased after

VBCP2.5 stimulation ( $p$  < 0.01). Results showed that VBCP2.5 was able to promote cytokine secretion in macrophages.

## 4. Discussion

Nano-biomaterials show great potential in immune regulation. When nanomaterials enter the body, their surface properties will change dynamically, resulting in immune activation or inhibition. This is an important information, which is helpful to understand the mechanism of immune response induced by polysaccharides. However, studies on such properties and immune activity of polysaccharides have not been well reported.

This study, we purified a homogeneous polysaccharide from VBRB. We firstly revealed its micelle formability and

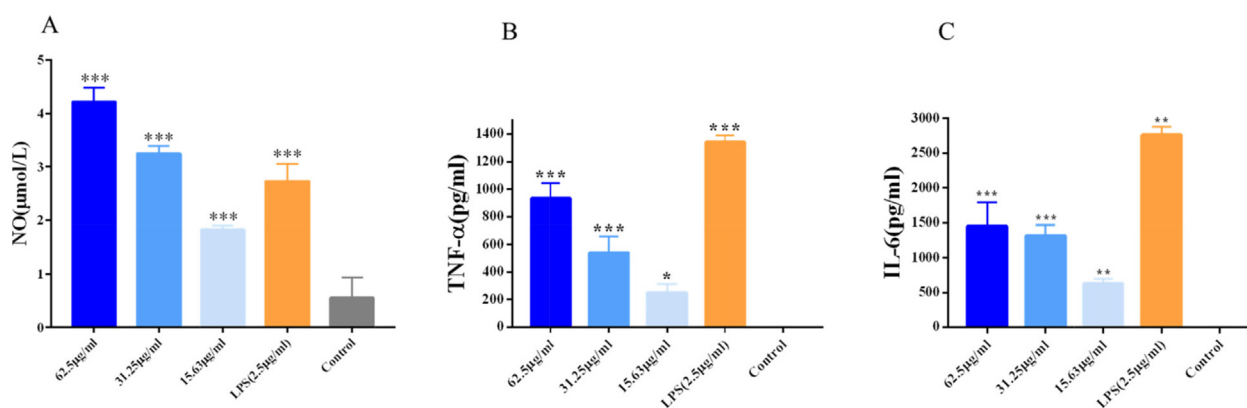


**Fig. 7** VBCP2.5 promoted NO release and cytokine secretion of macrophages. **A.** Effects of VBCP2.5 on NO release; **B** and **C.** cytokines secretion of Raw 264.7. Data were expressed as the means  $\pm$  SD ( $n = 3$ ) and significances with control group were presented as \* $p$  < 0.05 and \*\*,  $p$  < 0.01; \*\*\* $p$  < 0.001.

nano-properties. Tyndall phenomenon indicated that VBCP2.5 might form aggregates in solution. Fluorescence measurements in the presence of a fluorophore like Py can supply valuable information about the ability of an amphiphilic compound to form aggregates (Nichifor et al., 2014). Currently, polysaccharides or polysaccharides derived nanoparticles are synthesized by different mechanisms (e.g., polyelectrolyte, complexation, self-assembly, covalent cross-linking and ionic cross-linking), depending on the properties of polysaccharides (Debele et al., 2016). A lower CMC value indicated a higher self-association capacity of VBCP2.5 without any modification, which suggested a natural structure advantage. This may result from ionic linkage, between two carboxyl groups belonging to two different chains in close contact with each other, or the cross-linking, involves a combination of hydrogen bonds and hydrophobic interactions between the molecules (Debele et al., 2016). The microenvironment in contact with nanoparticles influences their surface dynamics, which in turn determines the functional response. VBCP2.5 had a main size peak of  $\sim 314.40$  nm in deionized water, while a main peak of  $\sim 84.99$  nm in simulated bloodfluid was recorded. This was most likely related to VBCP2.5 surface interaction dynamics with biomolecules, leading to the formation of a "protein corona" that lowers the surface energy and modifies its surface in terms of chemical composition and physicochemical interactions. When VBCP2.5 was incubated in deionized water for 24 h at the same temperature, the main peak was recorded at  $146.40 \pm 11.08$  nm. This may indicate that the particle size of VBCP2.5 in general environment was a dynamic equilibrium process, which was affected by temperature and tend to be stable with the extension of time. There was no obvious change after incubation for 1 h and 24 h in simulated bloodfluid, which may be due to the interplay between protein and VBCP2.5 was a quick dynamic equilibrium process of binding and unbinding. In both cases, VBCP2.5 characterized by small distribution of size, with PDI  $> 0.08$ . Generally, the charge value of polysaccharide can be indicative of the stability in solution and the negative charge was mainly produced by the uronic acid (Gu et al., 2020), that could be used to explain its negative charge in an aqueous solution. In contact with body fluids, nanoparticles can undergo significant surface changes. Positive value was measured after incubation in simulated bloodfluid for 1 h and 24 h, may due to the polymer-protein stronger interaction. Scanning electron microscopy can be used to observe the ultrastructure of macromolecules. The formation of irregular aggregation such as spheroid, flake and dendrimer indicated the complexity and flexibility of VBCP2.5, which may be related to the high purity, the size of carbohydrate chain and the strong intermolecular interaction (Shu-Jie et al., 2019). The cracks on the surface of the polymer were observed at magnification of  $15000\times$ , which may be due to the repulsions between the polysaccharide's molecules and the weak intermolecular attraction. Protrusions and folds were observed on the enlarged surface of the polymer of VBCP2.5, which most related to the adhesiveness of polysaccharides in solution. The structure analysis showed that VBCP2.5 was an acidic polysaccharide with a molecular weight of 674 kDa. VBCP2.5 characterized by high proportion of 1,4 linked- $\alpha$ -D-GalpA and a small fraction of RG-I covalently linked with 1,5 linked- $\alpha$ -L-Araf as backbone, 1,5 linked- $\alpha$ -L-Araf as side chain attached to the backbone, and terminal saccharides consisted of t- $\alpha$ -L-

Araf, t- $\beta$ -D-Glcp and t- $\alpha$ -D-Galp. Most of reported Radix Bupleuri polysaccharides mainly composed of galacturonic acid, galactose, glucose, arabinose, xylose, ribose and rhamnose (Jiang et al., 2020). Molecular weights ranging from 8 kDa  $\sim >2000$  kDa (Hy et al., 2013; Chuanhuan et al., 1995). The common linked residues such as terminal, 1, 6-linked, 1, 3-linked and 1, 3, 6-linked Glcp, terminal, 1, 5 and 1,3,5-linked Araf, terminal, 1, 4-linked, 1, 6-linked and 1, 4, 6-linked Galp, terminal, and, 1, 4-linked and 1, 4, 6-linked Manp and so on<sup>47</sup>. Zhao Y et al. (Zhao et al., 2020) obtained a homogeneous acidic heteropolysaccharide VBCP3-A from VBRB with a molecular weight of 963 kDa. Its monosaccharides composed of rhamnose, arabinose, galactose and galacturonic acid at a molar ratio of 1.00:2.39:0.98:5.93. The main linkages of the residues of VBCP3-A include 1,5-linked- $\alpha$ -L-Araf, 1,3,5-linked- $\alpha$ -L-Araf, and 1,4- $\beta$ -D-GalA. To the best of our knowledge, structure characterization of VBCP2.5 was different from previous reported polysaccharides of Radix bupleuri.

The composition analysis showed that the endotoxin content of VBCP2.5 was  $< 1.5$  EU/mL. Thus, other interference of immunomodulation could be excluded (Schepetkin and Quinn, 2006). Experiments in vitro showed that VBCP2.5 could promote the phagocytosis, the NO release, the TNF- $\alpha$  and IL-6 secretion of RAW264.7 cells which indicated the significant immune-enhancing function. Phagocytosis is a primary indicator of macrophage activation and plays an important role in the non-specific immune responses of the body (Pan et al., 2017). NO is a gaseous signalling molecule with anti-bacterial host defense function (Ramachandran et al., 2018). TNF- $\alpha$  can be involved in the defense against bacteria and virus, and IL 6 is a pleiotropic cytokine with wide effects within the integrated immune response (Rose-John et al., 2017). The first reported immune-related polysaccharides are mainly bacterial lipopolysaccharide. LPS activates macrophages to produce a variety of mediators and inflammatory cytokines, which help control the growth and spread of invading pathogens effectively. However, the excessive and uncontrolled production of these mediators and inflammatory cytokines may lead to serious systemic complications. The production of NO, TNF- $\alpha$  and IL-6 stimulated by VBCP2.5 at the same dose is significantly lower than that of LPS, which mean that the immunoregulation of VBCP2.5 would not cause excessive production of mediators and inflammatory cytokines.

Provided evidences concluded that VBCP2.5 was a polysaccharide with characteristics of nanoscale and nanostructure, which exhibit a good immune enhancement effect. Beside the primary structure, properties including size, surface charge, shape and deformability also affect interactions with immune cells (Perciani et al., 2021). Nanomaterials are easily recognized phagocytosed by macrophages, subsequent an immune response. Phagocytosis is the primary mechanism for nanoparticles uptake by macrophages. Varying nanoparticles' size and shape impact their mechanism of uptake, ability to accumulate in immune cells. For smaller size of  $20 \sim 500$  nm, both clathrin-dependent and clathrin-independent mechanisms are primarily involved (Boraschi et al., 2017). The positive charged surface will promote the internalization rate and further increase the internalization amount, compared with their negative counterparts, owing to the electrostatic interaction occurring with negatively charged cell membrane (Salatin and Yari, 2017). Compared with rigid particles, soft particles are more

easily deformed by cells during phagocytosis. This deformation can lead to local changes in the shape and orientation of the ligand molecule, making the internalization process less energetically favorable (Si et al., 2021).

Based on the above cognition, we discussed possible immune response mechanism activated by VBCP2.5. The activation of macrophages may through endocytosis pathway and clathrin may involve in this process. The positive charge on surface and the characteristics of flexible chain may contribute to this process. The spongy folds seen to be related to the adhesiveness of VBCP2.5 that could provide an opportunity to improve the residence time and to increase binding or uptake properties.

## 5. Conclusion

A polysaccharide with nano characteristic was isolated from Vinegar-baked Radix Bupleuri. It was an acidic polysaccharide with a molecular weight of 674 kDa and characterized by high proportion of 1,4 linked- $\alpha$ -D-GalpA and a small fraction of RG-I, Araf and Gal as side chain attached to the backbone, terminal saccharides included t- $\alpha$ -L-Araf, t- $\beta$ -D-Glcp and t- $\alpha$ -D-Galp. More importantly, this polysaccharide with a small size and positive charge of surface in stimulated blood fluid, as well as possessed flexible conformation, exhibited beneficial immunomodulation function in Raw264.7. The possible activation of macrophages by VBCP2.5 may be mediated through endocytosis pathway. The results in this work proposes new insights for the correlation between nano-properties of polysaccharides and the immune responses induced.

## Declaration of Competing Interest

The authors declare that they have no known competing financial interests or personal relationships that could have appeared to influence the work reported in this paper.

## Acknowledgments

This work was financially supported by the National Natural Science Foundation of China (82173981, 82074086, 81573612).

## Appendix A. Supplementary data

Supplementary data to this article can be found online at <https://doi.org/10.1016/j.arabjc.2022.104008>.

## References

- Boraschi, D., Italiani, P., Palomba, R., Decuzzi, P., Duschl, A., Fadeel, B., Moghimi, S.M., 2017. Nanoparticles and innate immunity: new perspectives on host defence. *Semin. Immunol.* 2017, 33–51. <https://doi.org/10.1016/j.smim.2017.08.013>.
- Cant, A., Cole, T., 2010. Infections in the immunocompromised. *Adv. Exp. Med. Biol.* 2010, 1–18. <https://doi.org/10.1007/978-1-4419-0981-7-1>.
- Cardoso, S.M., Silva, A.M., Coimbra, M.A., 2002. Structural characterisation of the olive pomace pectic polysaccharide arabinan side chains. *Carbohydr. Res.* 2002, 917–924. [https://doi.org/10.1016/S0008-6215\(02\)00082-4](https://doi.org/10.1016/S0008-6215(02)00082-4).
- Cheng, X.Q., Li, H., Yue, X.L., Xie, J.Y., Zhang, Y.Y., Di, H.Y., Chen, D.F., 2010. Macrophage immunomodulatory activity of the polysaccharides from the roots of *Bupleurum smithii* var. *parvifolium*. *J. Ethnopharmacol.* 2010, 363–368. <https://doi.org/10.1016/j.jep.2010.05.019>.
- Chuanhuan, L., Zuohua, W., Lunong, C., 1995. Experimental study on radiation resistance of *Bupleurum* polysaccharide. *Chin. Traditional Herbal Drugs* 1995, 645–646.
- Debele, T.A., Mekuria, S.L., Tsai, H.C., 2016. Polysaccharide based nanogels in the drug delivery system: Application as the carrier of pharmaceutical agents. *Mater. Sci. Eng. C Mater. Biol. Appl.* 2016, 964–981. <https://doi.org/10.1016/j.msec.2016.05.121>.
- Fang-bo, Y.A.N.G., Hui, G.O.N.G., Yi-ping, L.I.U., 2017. Effect of immunopotentiators on the prevention and treatment of infection. *Central South Pharmacy* 2017, 483–486.
- Fauci, A.S., Touchette, N.A., Folkers, G.K., 2005. Emerging infectious diseases: a 10-year perspective from the National Institute of Allergy and Infectious Diseases. *Emerg. Infect. Dis.* 2005, 519–525. <https://doi.org/10.3201/eid1104.041167>.
- Feiwu, L., Zishan, W., Zhen, R., Chunyu, T., Jia, H., Weili, H.e., Xiao, L.i., Bo, Q., Yange, Z., Qing, L., Run, Z., Jia, L., 2020. Pharmacological action, chemical constituents, development and utilization of *Bupleurum*. *Asia-Pacific Traditional Med.* 2020, 202–205.
- Gan, L., Li, X., Zhang, H., Zhang, R., Wang, H., Xu, Z., Peng, B., Tian, Y., 2020. Preparation, characterization and functional properties of a novel exopolysaccharide produced by the halophilic strain *Halomonas saliphila* LCB169(T). *Int. J. Biol. Macromol.* 2020, 372–380. <https://doi.org/10.1016/j.ijbiomac.2020.04.062>.
- Gu, J., Zhang, H., Yao, H., Zhou, J., Duan, Y., Ma, H., 2020. Comparison of characterization, antioxidant and immunological activities of three polysaccharides from *Sagittaria sagittifolia* L. *Carbohydr. Polym.* 2020. [https://doi.org/10.1016/j-carbpol.2020.115939](https://doi.org/10.1016/j.carbpol.2020.115939) 115939.
- He, P.F., He, L., Zhang, A.Q., Wang, X.L., Qu, L., Sun, P.L., 2017. Structure and chain conformation of a neutral polysaccharide from sclerotia of *Polyporus umbellatus*. *Carbohydr. Polym.* 2017, 61–67. <https://doi.org/10.1016/j.carbpol.2016.08.041>.
- Hy, D.I., Zhang, Y.Y., Chen, D.F., 2013. Isolation of an anti-complementary polysaccharide from the root of *Bupleurum chinense* and identification of its targets in complement activation cascade. *Chin. J. Nat. Med.* 2013, 177–184. [https://doi.org/10.1016/S1875-5364\(13\)60046-1](https://doi.org/10.1016/S1875-5364(13)60046-1).
- Jiang, H., Yang, L., Hou, A., Zhang, J., Wang, S., Man, W., Zheng, S., Yu, H., Wang, X., Yang, B., Wang, Q., Kuang, H., 2020. Botany, traditional uses, phytochemistry, analytical methods, processing, pharmacology and pharmacokinetics of *Bupleuri Radix*: A systematic review. *Biomed. Pharmacother.* 2020. <https://doi.org/10.1016/j.biopha.2020.110679> 110679.
- Khan, I., Saeed, K., Khan, I., 2019. Nanoparticles: Properties, applications and toxicities. *Arab. J. Chem.* 2019, 908–931.
- Lasola, J.J.M., Kamdem, H., McDaniel, M.W., Pearson, R.M., 2020. Biomaterial-Driven Immunomodulation: Cell Biology-Based Strategies to Mitigate Severe Inflammation and Sepsis. *Front. Immunol.* 2020, 1726. <https://doi.org/10.3389/fimmu.2020.01726>.
- Li, L.F., Wong, T.L., Han, Q.B., 2019. Difficulties in research of Chinese medicine polysaccharides. *Chin. J. Nat. Med.* 2019, 883–886. [https://doi.org/10.1016/S1875-5364\(19\)30107-4](https://doi.org/10.1016/S1875-5364(19)30107-4).
- Lihong, Z., 2015. The application analysis of immunoenhancer oral formulations in children hospital outpatient. *Chin. J. Clin. Rational Drug Use* 2015, 30–31.
- Liu, Z., Jiao, Y., Wang, Y., Zhou, C., Zhang, Z., 2008. Polysaccharides-based nanoparticles as drug delivery systems. *Adv. Drug Deliv. Rev.* 2008, 1650–1662. <https://doi.org/10.1016/j.addr.2008.09.001>.
- Medina, K.L., 2016. Overview of the immune system. *Handb. Clin. Neurol.* 2016, 61–76. <https://doi.org/10.1016/B978-0-444-63432-0.00004-9>.
- Mohnen, D., 2008. Pectin structure and biosynthesis. *Curr. Opin. Plant Biol.* 2008, 266–277. <https://doi.org/10.1016/j.pbi.2008.03.006>.

- Nichifor, M., Mocanu, G., Stanciu, M.C., 2014. Micelle-like association of polysaccharides with hydrophobic end groups. *Carbohydr. Polym.* 2014, 209–218. <https://doi.org/10.1016/j.carbpol.2014.03.072>.
- Nii-Trebi, N.I., 2017. Emerging and Neglected Infectious Diseases: Insights, Advances, and Challenges. *Biomed. Res. Int.* 2017, 5245021. <https://doi.org/10.1155/2017/5245021>.
- Padmanabhan, A., Shah, N.P., 2020. Structural characterization of exopolysaccharide from *Streptococcus thermophilus* ASCC 1275. *J. Dairy Sci.* 2020, 6830–6842. <https://doi.org/10.3168/jds.2019-17439>.
- Pan, G., Xie, Z., Huang, S., Tai, Y., Cai, Q., Jiang, W., Sun, J., Yuan, Y., 2017. Immune-enhancing effects of polysaccharides extracted from *Lilium lancifolium* Thunb. *Int. Immunopharmacol.* 2017, 119–126. <https://doi.org/10.1016/j.intimp.2017.08.030>.
- Parkin, J., Cohen, B., 2001. An overview of the immune system. *Lancet* 2001, 1777–1789. [https://doi.org/10.1016/S0140-6736\(00\)04904-7](https://doi.org/10.1016/S0140-6736(00)04904-7).
- Perciani, C.T., Liu, L.Y., Wood, L., MacParland, S.A., 2021. Enhancing Immunity with Nanomedicine: Employing Nanoparticles to Harness the Immune System. *ACS Nano* 2021, 7–20. <https://doi.org/10.1021/acsnano.0c08913>.
- Ramachandran, R.A., Lupfer, C., Zaki, H., 2018. The Inflammasome: Regulation of Nitric Oxide and Antimicrobial Host Defence. *Adv. Microb. Physiol.* 2018, 65–115. <https://doi.org/10.1016/bs.ampbs.2018.01.004>.
- Rose-John, S., Winthrop, K., Calabrese, L., 2017. The role of IL-6 in host defence against infections: immunobiology and clinical implications. *Nat. Rev. Rheumatol.* 2017, 399–409. <https://doi.org/10.1038/nrrheum.2017.83>.
- Ruibin, B., Ma, Y.-L., Pei, Z., Yanping, W., Dong, L.Y., Fangdi, H. u., 2017. Content Determination of Saccharide in Polysaccharides Containing Galacturonic Acid by Phenol-sulfuric Acid Method Combined with Calibration Factor Method. *China Pharm.* 2017, 2974–2978.
- Salatin, S., Yari, K.A., 2017. Overviews on the cellular uptake mechanism of polysaccharide colloidal nanoparticles. *J. Cell Mol. Med.* 2017, 1668–1686. <https://doi.org/10.1111/jcmm.13110>.
- Schepetkin, I.A., Quinn, M.T., 2006. Botanical polysaccharides: macrophage immunomodulation and therapeutic potential. *Int. Immunopharmacol.* 2006, 317–333. <https://doi.org/10.1016/j.intimp.2005.10.005>.
- Serrano-Sevilla, I., Artiga, A., Mitchell, S.G., De Matteis, L., de la Fuente, J.M., 2019. Natural Polysaccharides for siRNA Delivery: Nanocarriers Based on Chitosan, Hyaluronic Acid, and Their Derivatives. *Molecules* 2019. <https://doi.org/10.3390/molecules24142570>.
- Shi, Y., Ye, Y.F., Zhang, B.W., Liu, Y., Wang, J.H., 2021. Purification, structural characterization and immunostimulatory activity of polysaccharides from *Umbilicaria esculenta*. *Int. J. Biol. Macromol.* 2021, 743–751. <https://doi.org/10.1016/j.ijbiomac.2021.03.176>.
- Shu-Jie, Z.H.A.N.G., Wei, Q.U.A.N., Hong-Wei, J.I.A.N.G., Yu-Fan, K.A.N.G., 2019. Analysis of the Polysaccharides with Different Purification Levels in Pea (*Pisum sativum*) by Scanning Electron Microscope. *J. Agric. Biotechnol.* 2019, 1822–1830.
- Si, Y., Luo, H., Zhou, F., Bai, X., Han, L., Sun, H., Cha, R., 2021. Advances in polysaccharide nanocrystals as pharmaceutical excipients. *Carbohydr. Polym.* 2021. <https://doi.org/10.1016/j.carbpol.2021.117922> 117922.
- Stone, J.K., Heiss, C., Wang, Z., Black, I., Grasso, S.A., Koppisch, A. T., Azadi, P., Keim, P., Tuanyok, A., 2014. Structural characterization of polysaccharides expressed by *Burkholderia oklahomensis* E0147. *Carbohydr. Res.* 2014, 68–72. <https://doi.org/10.1016/j.carres.2013.08.011>.
- Sun, P., Li, Y., Wei, S., Zhao, T., Wang, Y., Song, C., Xue, L., Wang, F., Xiao, L., Wu, J., Qiao, M., 2019. Pharmacological Effects and Chemical Constituents of *Bupleurum*. *Mini Rev. Med. Chem.* 2019, 34–55. <https://doi.org/10.2174/1871520618666180628155931>.
- Tang, C., Sun, J., Liu, J., Jin, C., Wu, X., Zhang, X., Chen, H., Gou, Y., Kan, J., Qian, C., Zhang, N., 2019. Immune-enhancing effects of polysaccharides from purple sweet potato. *Int. J. Biol. Macromol.* 2019, 923–930. <https://doi.org/10.1016/j.ijbiomac.2018.11.187>.
- Toamih, A.H., Abu, A.N., Iraqi, F.A., 2018. The Collaborative Cross mouse model for dissecting genetic susceptibility to infectious diseases. *Mamm. Genome* 2018, 471–487. <https://doi.org/10.1007/s00335-018-9768-1>.
- Toma, C.C., Aloisi, A., Bordoni, V., Di Corato, R., Rauner, M., Cuniberti, G., Delogu, L.G., Rinaldi, R., 2018. Immune Profiling of Polysaccharide Submicron Vesicles. *Biomacromolecules* 2018, 3560–3571. <https://doi.org/10.1021/acs.biomac.8b00832>.
- Torres, F.G., Troncoso, O.P., Pisani, A., Gatto, F., Bardi, G., 2019. Natural Polysaccharide Nanomaterials: An Overview of Their Immunological Properties. *Int. J. Mol. Sci.* 2019. <https://doi.org/10.3390/ijms20205092>.
- Wang, Y., Guo, M., 2020. Purification and structural characterization of polysaccharides isolated from *Auricularia cornea* var. *Li*. *Carbohydr. Polym.* 2020. [https://doi.org/10.1016/j-carbpol.2019.115680](https://doi.org/10.1016/j.carbpol.2019.115680) 115680.
- Weber, D.J., Rutala, W.A., 2003. Immunization of immunocompromised persons. *Immunol. Allergy Clin. North Am.* 2003, 605–634. [https://doi.org/10.1016/s0889-8561\(03\)00100-0](https://doi.org/10.1016/s0889-8561(03)00100-0).
- Wenbo, L.v., Shuang, W., Yang, Y.e., 2015. Research progress of Chinese medicine immune enhancer. *J. Heilongjiang Ecological Eng. Vocational College* 2015, 17–18.
- Wilson, R.H., Smith, A.C., Kacurakova, M., Saunders, P.K., Wellner, N., Waldron, K.W., 2000. The mechanical properties and molecular dynamics of plant cell wall polysaccharides studied by Fourier-transform infrared spectroscopy. *Plant Physiol.* 2000, 397–405. <https://doi.org/10.1104/pp.124.1.397>.
- Wu, F., Zhou, C., Zhou, D., Ou, S., Zhang, X., Huang, H., 2018. Structure characterization of a novel polysaccharide from *Hericium erinaceus* fruiting bodies and its immunomodulatory activities. *Food Funct.* 9 (1), 294–306.
- Xia, Y.G., Huang, Y.X., Liang, J., Kuang, H.X., 2020. Comparable studies of two polysaccharides from leaves of *Acanthopanax senticosus*: Structure and antioxidant. *Int. J. Biol. Macromol.* 2020, 350–362. <https://doi.org/10.1016/j.ijbiomac.2019.12.244>.
- Xie, J.H., Jin, M.L., Morris, G.A., Zha, X.Q., Chen, H.Q., Yi, Y., Li, J.E., Wang, Z.J., Gao, J., Nie, S.P., Shang, P., Xie, M.Y., 2016. Advances on Bioactive Polysaccharides from Medicinal Plants. *Crit. Rev. Food Sci. Nutr.* 2016, S60–S84. <https://doi.org/10.1080/10408398.2015.1069255>.
- Xu, Y., Dong, Q., Qiu, H., Ma, C.W., Ding, K., 2011. A homogalacturonan from the radix of *Platycodon grandiflorum* and the anti-angiogenesis activity of poly-/oligogalacturonic acids derived therefrom. *Carbohydr. Res.* 2011, 1930–1936. <https://doi.org/10.1016/j.carres.2011.05.011>.
- Xueqin, W.A.N.G., Yang, Z.H.A.O., Xinti, W.A.N.G., Xuejiao, Z.H. A.O., Jiyan, C.H.E.N., 2018. Research progress on chemical constituents and pharmacological actions of vinegar-baked Radix Bupleuri. *Drug Evaluation Res.* 2018, 163–168.
- Yaping, L.i., Hongli, Z., 2019. Progress in the determination of uronic acid in polysaccharides. *Food Res. Develop.* 2019, 207–211.
- Zeng, H., Huang, L., Tao, H., Zhang, Y., Ding, K., 2020. Structural elucidation of a pectin from roots of *Polygala tenuifolia* and its neuritogenesis inducing activity in PC12 cells. *Carbohydr. Polym.* 2020. <https://doi.org/10.1016/j.carbpol.2020.116048> 116048.
- Zhang, S., Li, Z., Wang, X., An, L., Bao, J., Zhang, J., Cui, J., Li, Y., Jin, D.Q., Tuerhong, M., Abudukeremu, M., Ohizumi, Y., Xu, J., Guo, Y., 2020. Isolation, structural elucidation, and immunoregulation properties of an arabinofuranan from the rinds of *Garcinia mangostana*. *Carbohydr. Polym.* 2020. <https://doi.org/10.1016/j.carbpol.2020.116567> 116567.

- Zhang, M., Wu, W., Ren, Y., Li, X., Tang, Y., Min, T., Lai, F., Wu, H., 2017. Structural Characterization of a Novel Polysaccharide from *Lepidium meyenii* (Maca) and Analysis of Its Regulatory Function in Macrophage Polarization in Vitro. *J. Agric. Food Chem.* 2017, 1146–1157. <https://doi.org/10.1021/acs.jafc.6b05218>.
- Zhang, Y., Zhou, T., Wang, H., Cui, Z., Cheng, F., Wang, K.P., 2016. Structural characterization and in vitro antitumor activity of an acidic polysaccharide from *Angelica sinensis* (Oliv.) Diels. *Carbohydr. Polym.* 2016, 401–408. <https://doi.org/10.1016/j.carbpol.2016.04.002>.
- Zhao, Y., Wan, P., Wang, J., Li, P., Hu, Q., Zhao, R., 2020. Polysaccharide from vinegar baked radix bupleuri as efficient solubilizer for water-insoluble drugs of Chinese medicine. *Carbohydr. Polym.* 2020., <https://doi.org/10.1016/j.carbpol.2019.115473> 115473.
- Zhao, Y., Yan, B., Wang, Z., Li, M., Zhao, W., 2020. Natural Polysaccharides with Immunomodulatory Activities. *Mini Rev. Med. Chem.* 2020, 96–106. <https://doi.org/10.2174/1389557519666190913151632>.